Volume 1 | Number 1 | Jan 2013 | Pages 1–100

Dalton
Transactions

An international journal of inorganic chemistry
www.rsc.org/dalton

ROYAL SOCIETY
OF CHEMISTRY

This is an *Accepted Manuscript*, which has been through the Royal Society of Chemistry peer review process and has been accepted for publication.

Accepted Manuscripts are published online shortly after acceptance, before technical editing, formatting and proof reading. Using this free service, authors can make their results available to the community, in citable form, before we publish the edited article. We will replace this *Accepted Manuscript* with the edited and formatted *Advance Article* as soon as it is available.

You can find more information about *Accepted Manuscripts* in the **Information for Authors**.

Please note that technical editing may introduce minor changes to the text and/or graphics, which may alter content. The journal's standard **Terms & Conditions** and the **Ethical guidelines** still apply. In no event shall the Royal Society of Chemistry be held responsible for any errors or omissions in this *Accepted Manuscript* or any consequences arising from the use of any information it contains.

Journal Name

ARTICLE

New Amide-Chloride Phases in the Li-Al-N-H-Cl System: Formation and Hydrogen Storage Behaviour

L. Fernández Albanesi[a], S. Garroni[b], S. Enzo[b] and F. C. Gennari[a*]

New amide-chloride phases were successfully synthesized by mechanical milling of the $LiNH_2$-$AlCl_3$ mixture at a molar ratio of 1:0.11 and further heating at 150 ºC under argon (0.1 MPa) or under hydrogen pressure (0.7 MPa). Powder X-ray diffraction measurements as a function of milling time increase revealed that the milling of the $LiNH_2$-$0.11AlCl_3$ mixture conducts to the formation of a FCC solid solution with excess of $LiNH_2$. Posterior heating of the $LiNH_2$-$0.11AlCl_3$ sample ball milled for 5 hours at 150 ºC under argon or under hydrogen induces the apparition of an amide-chloride phase isostructural with cubic $Li_4(NH_2)_3Cl$. This Li-Al-N-H-Cl phase transforms progressively into the trigonal phase after prolonged heating at 300 ºC under hydrogen pressure. The thermal behaviour of the amide-chloride without and with LiH addition displays dissimilar decomposition pathways. The decomposition of amide-chloride alone involves the formation of ammonia and hydrogen from 120 to 300 ºC. Conversely, amide-chloride material in presence of LiH only releases hydrogen avoiding the emmision of ammonia. The resultant material is able to be rehydrogenated under moderate conditions (300 ºC, 0.7 MPa H_2), providing a new reversible hydrogen storage system.

Introduction

Hydrogen storage in solids is considered a practical and promising approach for onboard applications owing to its high volumetric efficiency and comparatively safe operating conditions.[1] Requirements for high capacity hydrogen storage materials have addressed the attention in developing novel complex hydrides or multi-component hydrides with light elements.[2-4] In particular, the Li-N-H system is able to reversibly desorb/absorb hydrogen according with the reaction:[2]

$$LiNH_2(s) + LiH(s) \leftrightarrow Li_2NH(s) + H_2(g) \qquad (1)$$
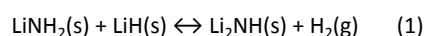
with a theoretical hydrogen storage of 6.5 wt%. Two independent studies[5,6] have proposed that the hydrogen desorption reaction (1) proceeds through the following two-step elementary reaction mediated by ammonia:

$$2LiNH_2(s) \rightarrow Li_2NH(s) + NH_3(g) \qquad (2)$$

$$NH_3(g) + LiH(s) \leftrightarrow LiNH_2(s) + H_2(g) \qquad (3)$$
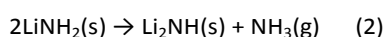
First, $LiNH_2$ decomposes releasing NH_3, which quickly reacts with LiH to form $LiNH_2$ again and liberates hydrogen. The adequate mixing of $LiNH_2$ with LiH and the use of an excess of LiH avoid the releasing of ammonia, which causes the system to decrease its storage capacity.[7,8]

Unfortunately, the operating temperature for dehydrogenation of the $LiNH_2$-LiH mixture is still superior to 250 °C at 1 bar due to kinetic and/or thermodynamic restrictions. In fact, the theoretical enthalpy change calculated[2] for reaction (1) is -40 $kJ.molH_2^{-1}$ whereas the measured[9,10] value is about -66 $kJ.molH_2^{-1}$. One approach to modifying the thermodynamic stability of the $LiNH_2$-LiH composite and improving its hydrogen storage properties, is by substituting Li^+ and/or $[NH_2]^-$ for other ionic groups. Reduction in the decomposition temperature of $LiNH_2$ by cation/anion doping was reported by using halides.[11-20] Zhang et al.[11] proposed that the interaction between a chlorine ion of LiCl with $LiNH_2$ weakens the bond between Li^+ and $[NH_2]^-$. Leng et al.[12] showed that depending on the $MgCl_2$ amount added to $LiNH_2$, the operating dehydriding mechanism is different. In that context, the role of $MgCl_2$ changed from a simple NH_3 sorbent ($MgCl_2$ < 4 mol%) or a compound able to form a solid solution with $LiNH_2$ ($MgCl_2$ >4 mol%) to an additive that produced the $LiNH_2$-LiH-$0.5Mg(NH_2)_2$ composite. Moreover, simultaneous cation and anion doping was explored by Anderson et al.,[13-15] who found a wide range of new amide halide phases $Li_{1+m}(NH_2)X_m$ and $LiMg_n(NH_2)X_{2n}$ (where X = Cl, Br, I) that released

a. Consejo Nacional de Investigaciones Científicas y Técnicas (CONICET), Centro Atómico Bariloche (CNEA) and Instituto Balseiro (UNCu), Av. Bustillo 9500 R8402AGP Bariloche, Río Negro, Argentina. E-mail: gennari@cab.cnea.gov.ar; Tel.: +54 294 4445118; Fax: +54 294 4445190
b. Department of Chemistry and Pharmacy, University of Sassari and INSTM, Via Vienna 2, I-07100 Sassari, Italy.
†Electronic Supplementary Information (ESI) available: [T1. Phase abundance, crystallite sizes and cell parameters of the LA sample after different times of B.M.; S1. XRPD patterns of LA and LLA samples after 5 h of BM; S2. XRPD patterns of $LiNH_2$:1.6LiH:$0.11AlCl_3$ after different times of BM; S3. EDS analysis of LA sample after different thermal treatments; S4. TG and DTG curves of LA and LLA samples. S5. FTIR gas analysis of the species released during LA decomposition; S6. FTIR spectra after non-isothermal heating at 300 ºC for LA and LLA samples; S7. Hydrogen desorption and absorption of LLA at 300 ºC].

hydrogen reversibly and with undetectable NH_3 emission. It was shown that the addition of lithium halides to $LiNH_2$ reduced the dehydrogenation temperature and suppressed the emission of ammonia. An extra reduction in the dehydrogenation temperature was obtained when magnesium halides were added to the Li-N-H system. Preliminary conductivity measurements showed a direct relation between the ionic conductivities of the amide halide materials and the dehydriding/rehydriding rates on heating.[13-15] This evidence is in agreement with previous studies,[16] where the diffusion of Li^+ into and H^+ out of the face centred cubic anion lattice or vice versa was highlighted as a key factor for a direct/reverse reaction (1).

The addition of lithium halides to amides was explored,[17-24] with the aim to improve these hydrogen storage systems via in-situ formation of lithium fast-ion conductors. Li *et al.* reported the formation of $Li_7(NH_2)_6Br$ phase by LiBr addition, which is supposed to weaken the N-H bond and also to promote the migration of Li^+.[17] In the case of LiCl addition to $Mg(NH_2)$-2LiH, a complex dehydrogenation process was observed with respect to the un-doped sample, but the onset temperature of dehydrogenation remained almost the same. Comparatively, LiBr was the best additive among all lithium halides, which induced significant improvement in the dehydrogenation/rehydrogenation rates of the $Mg(NH_2)$-2LiH composite.[17] Specifically, LiBr reacted with $LiNH_2$ forming $Li_3(NH)Br$, which changed the reaction pathway and the reaction enthalpy of the system.[20,21] Recently, a negative effect of the LiCl addition to the $Mg(NH_2)_2$-2LiH composite was presented.[24] The formation in-situ of $Li_4(NH_2)_3Cl$ during hydrogen cycling at 200 °C deteriorated the hydrogen storage capacity and dehydrogenation rate due to the consumption of $LiNH_2$ by a competitive reaction. Our recent work proved that the addition of $AlCl_3$ (1.14 mol%) to $LiNH_2$:1.6LiH also enhances its hydrogen storage properties due to the incorporation to Al^{3+} and Cl^- into Li_2NH-type structure.[22] In fact, a stable hydrogen storage capacity of about 4.5-5.0 wt% was observed under cycling at 275 ºC and hydrogen was completely desorbed in 30 min avoiding the release of ammonia. In a further study using high $AlCl_3$ content (2.98 and 4.76 mol%), together with mild thermal treatments in controlled environments, we observed the formation of cubic and hexagonal amide-chloride phases in the Li-Al-N-H-Cl system by means of XRPD, FTIR and NMR measurements.[23] It was confirmed that these amide-chloride phases improve dehydrogenation properties compared to the $LiNH_2$-LiH, providing alternative reaction pathways.

From the above investigations, it is clear there is scope for further research on the addition of metal halides in the Li-N-H system. Furthermore, the amide-halide phase modifies the hydrogen storage performance of the material and more details are necessary to understand its formation mechanism. In this report, new amide-chloride phases in the Li-Al-N-H-Cl were synthesized from the mixture of $LiNH_2$-0.11$AlCl_3$ and structurally/thermally characterized using XRPD, FTIR, DSC, TG and volumetric measurements. The mixture of these amide-chloride phases and LiH provide a decomposition pathway alternative to that of pristine amide-

chloride, promoting the hydrogen release and affording a reversible hydrogen storage system.

Experimental

The starting materials were commercial $LiNH_2$ (Aldrich, 95%), LiH (Fluka, 95%) and anhydrous $AlCl_3$ (Merck, 98%). The sample preparation was carried out by ball milling (BM) of $LiNH_2$ and $AlCl_3$ in a 1:0.11 molar ratio. The milling procedure was performed by different milling times up to 5 h in a planetary type mill (Fritsch Pulverisette 6) under 0.1 MPa of an argon atmosphere, using 400 rpm with a ball/sample mass ratio of 40:1. The milled sample subjected to 5 h of BM was denoted with LA. For comparison purpose, the $LiNH_2$-LiH-$AlCl_3$ mixture with 1:1.6:0.11 molar ratio (4.06 mol% $AlCl_3$) was labelled as LLA, also obtained by 5 h of BM under similar experimental conditions of LA. The amount of LiH was added in excess respect to reaction (1) to avoid or minimize the formation of NH_3.[7,8] All samples were manipulated in an argon-filled glove box, with O_2 and H_2O levels < 1 ppm.

The LA sample was submitted to different thermal treatments under a hydrogen and argon atmosphere. A set of samples were heated at 150 or 300 °C under 0.7 MPa of hydrogen for 0.5, 1, 5 and 12 h. On the other hand, the LA sample was also heated at 150 °C under static argon at atmospheric pressure for 0.5 h. Structural information of the different samples was obtained by X-ray powder diffraction (XRPD) and Fourier transform infrared spectroscopy (FTIR). XRPD measurements were conducted on PANaytical Empyrean equipment (graphite monochromator) with Cu Kα radiation at 40 kV and 30 mA. The samples were mounted in an airtight holder to avoid any oxidation/hydrolysis process of the powders. Phase abundance and microstructural parameters were evaluated by fitting the XRPD patterns by Rietveld method using the software MAUD.[25,26] FTIR measurements were carried out using a spectrometer Perkin Elmer Spectrum 400. Selected samples were grounded with dry KBr under a purified argon atmosphere and pressed into pellets. Solid–state IR spectra were obtained in the range of 1000–4000 cm^{-1} using a specially designed cell, with a resolution of 4 cm^{-1}. Handling was done inside the glove box to avoid contact with air.

The thermal behaviour of LA and LLA samples was investigated by differential scanning calorimeter (DSC, TA 2910 calorimeter) and thermogravimetric analysis (TG, TA Instruments HP50 equipment) using argon (122 $ml.min^{-1}$) and helium (50 $ml.min^{-1}$) flow, respectively, with a heating rate of 5 $ºC.min^{-1}$. About 7-10 mg of sample were load into aluminium capsules closed in the glove box to avoid/minimize the exposure to air. Chemical analyses were performed via scanning electron microscopy (SEM) with an energy–dispersive X–ray spectrometer (EDS) analyser (SEM 230-Nova Nano and EDAX). Powder samples were dispersed on stick–mounted holders in the argon–filled glove box and introduced into hermetic plastic recipients to minimize the exposure to oxygen and humidity. Several analyses were performed on 1μm x 1μm zones. The values of Cl and Al atomic percentages were determined by EDS as an average of five measurements.

Dehydrogenation and hydrogenation kinetics were measured using a modified Sieverts-type device, coupled with a mass flow controller. The mass flow controller allows the determination of the amount of hydrogen supplied to the sample during the measurement, by means of an adequate calibration. If the mass flow controller is operated on a gas other than the one it was calibrated with (hydrogen), a correction factor has to be used to take into account the difference in heat capacities between the two gases. For isothermal measurements, the sample was heated up to 300 ºC under 0.7 MPa of hydrogen pressure and kept at this temperature for 30 min. Then, the sample was dehydrided (first desorption measurement) and consecutively rehydrided (first absorption measurement). Dehydriding experiments were conducted under non–isothermal conditions with constant heating rates of 5 ºC.min^{-1} under 0.02 MPa of hydrogen pressure. The amount of absorbed/desorbed hydrogen is reported as wt% respect to the total mass. The hydrogen amount was determined with a relative error <5%.

Results and discussion

Mechanical milling of LiNH$_2$ and AlCl$_3$: formation of the FCC solid-solution

Figure 1 displays the XRPD patterns of the LiNH$_2$-0.11AlCl$_3$ mixture after ball milling for different times. In Fig. 1A the bottom pattern highlights that the starting mixture is actually tetragonal LiNH$_2$ and monoclinic AlCl$_3$. After 5 minutes of BM, an unexpected solid state reaction occurs. In fact, AlCl$_3$ diffraction peaks disappear and the complete XRPD pattern could be decomposed according to 3 phases: the starting tetragonal LiNH$_2$, one cubic Li$_2$NH-type phase with lattice parameter 5.251 Å, and a second cubic phase with lattice parameter 5.149 Å. This latter phase can be attributed to the LiCl compound, space group $Fm\overline{3}m$. To evaluate clearly the progress of the solid state reaction, a magnification is shown in Fig.1B. In addition, Table T1 (ESI†) summarises the phase abundance obtained by Rietveld fitting and crystallite sizes of the main phases.


Figure 1. A. XRPD patterns of the LiNH$_2$-0.11AlCl$_3$ mixture after different times of milling. B. Detail in the angular range 2θ = 27-38. The green lines are the parametric representation of the background (Table T1, ESI†).

As milling time increases, only after 5 minutes, the intensity of the diffraction peaks of LiNH$_2$ significantly decreases and the formation of the two cubic Li$_2$NH-type and LiCl-type phases was clearly identified. These two cubic Li$_2$NH-type and LiCl-type phases can be recognized in the patterns of all specimens ball milled up to 1 h. The two parallel FCC sequences of peaks are shifted to 2θ positions lower than the values occurring for the stoichiometric Li$_2$NH imide on account of increased cubic lattice parameters. After 2 h of milling, mainly one metastable extended FCC solid solution with increased lattice parameter may be envisaged in the pattern; that is, this imide-like phase has incorporated the LiCl phase (with the same symmetry $Fm\overline{3}m$), whose peaks are located at systematically superior 2θ values. Such phase seems to coexist with a remaining contribution ascribable to a LiNH$_2$ phase. Further, precise location of the broadened peaks after indexing with the FCC hkl sequence supplies lattice parameter a = 5.231 Å after 5h of BM. The substantial line broadening observed for the FCC peaks may be ascribed to average crystallite size values of ca 180 Å, with an amount of internal strain of 0.0042 (Fig. S1, ESI†). Our final XRPD pattern after 5 h of milling can be described making reference to the structural model recently reported by Makepeace et al.[27] This model accounts for the presence of the hydrogen/deuterium atoms in a non-stoichiometric continuum between lithium amide and lithium imide making use of a basically FCC structure. The a × a × 2a tetragonal lithium amide structure was reduced into a cubic anti-fluorite Li$_2$NH cell, resulting in a unit cell with half-occupied lithium 8(c) sites and hydrogen/deuterium atoms in two disordered sites around the nitrogen atoms. Frenkel defects may be accommodated in non-occupied lithium sites obtained after symmetrisation of the LiNH$_2$ structure, translated and reduced to conform the $Fm\overline{3}m$ space group symmetry. From the pattern evolution shown in Figure 1, we can see that the tetragonal fingerprint of LiNH$_2$ dominating in the early stages of ball milling is leaving room for the $Fm\overline{3}m$ structure. Then, it is possible that not only Al^{3+} ions are accepted in the cation sites but that even the Cl$^-$ anions can be accommodated partially in some empty cavities, according to an equation of the type:
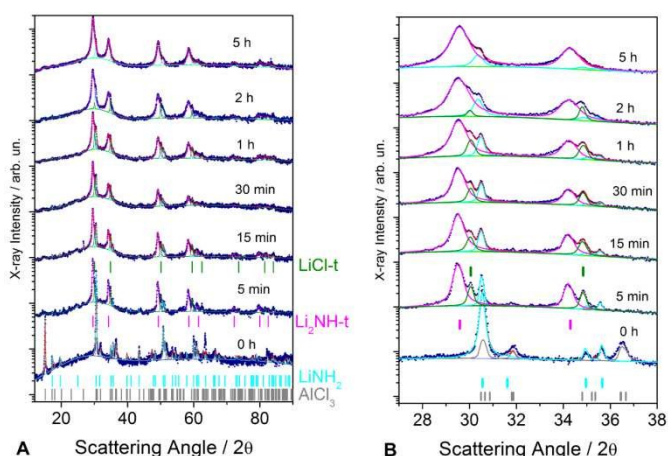
LiNH$_2$(s) + x AlCl$_3$(s) —milling→ LiAl$_x$(NH$_2$)Cl$_{3x}$(s)   (4)
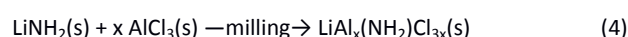
Makepeace et al.[27] proposed to accommodate the hydrogen species in general positions of high multiplicity corresponding to N-H bond length of 1.05 Å in a reference lattice parameter of 5.18 Å. Our observed lattice parameter of 5.231 Å suggests that Cl$^-$ anions may occupy even lower multiplicity sites just to fulfil the inter-atomic distances required according to the amount of AlCl$_3$ added in the mixture. Finally, the shoulders observed for some peaks in the pattern of Figure 1B may be explained with the presence of relatively low amounts of un-reacted LiNH$_2$ structure (see cyan line with the tetragonal contribution in the fit).

FTIR studies (Fig. 2) performed on LiNH$_2$-0.11AlCl$_3$ mixture after different milling times confirm the XRPD interpretations. In fact, the N-H asymmetric and symmetric stretching vibrations of LiNH$_2$ at 3315 and 3260 cm^{-1}, respectively[9], are observed as the milling time progresses up to 5 h. From the spectrum referred to specimen subjected to 5 min of milling, additional bands at 3297 and 3245 cm^{-1} associated with N-H vibrations are also seen. This may be
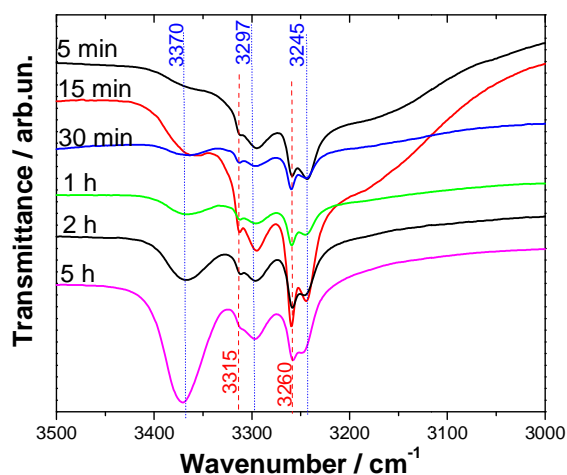
Figure 2. FTIR of the LiNH$_2$-0.11AlCl$_3$ mixture after different times of BM.

taken as evidence of the partial substitution of Li$^+$ by Al^{3+} ions in the Li$_4$(NH$_2$)$_3$Cl structure.[13] On the other hand, an extra band at 3370 cm^{-1} is clearly identified in the spectrum, which was previously associated with the presence of cation-coordinated NH$_3$ molecules.[28] The N-H bands at 3297 and 3245 cm^{-1} respectively could be related with amide formation due to their high wave numbers. Similar bands were recently ascribed to a new amide-chloride phase in the Li-Al-N-H-Cl system.[23]

When the LiNH$_2$-0.11AlCl$_3$ mixture is ball milled in the presence of LiH, the progress of reaction is similar to that showed in Fig. 1 (see Figure S2 ESI†). A solid-solid reaction is observed after 5 min of milling: the most intense peaks associated with AlCl$_3$ start to disappear while those corresponding to LiNH$_2$ decrease their intensity.

A progressive shift to lower 2θ positions with respect to LiNH$_2$ is observed with milling. After 5 h, we observe the formation of a FCC phase (Fig. S2, ESI†) with a lattice parameter a = 5.215 Å and crystallite size of 180 Å. The most intense peaks of LiH are also identified. Therefore, an analogous FCC solid solution is formed by the reaction between LiNH$_2$ and AlCl$_3$, independently of the LiH presence.

Thermal stability of FCC phase: formation of a new amide-chloride between LiNH$_2$ and AlCl$_3$

To address the thermal stability of the FCC solid solution, DSC curves of LiNH$_2$-0.11AlCl$_3$ and LiNH$_2$-1.6LiH-0.11AlCl$_3$ mixtures after 5 h of BM (LA and LLA samples) are displayed in Fig. 3. Two thermal events are clearly identified for LA and LLA samples: one of exothermic character at about 130 ºC and one endothermic at 275 or 235 ºC, depending on the presence of LiH. By comparison between the curves, it is possible to correlate the exothermic events with the interaction between LiNH$_2$ and AlCl$_3$, as it will be analysed below (see Fig. 4). On the other hand, the endothermic peak at higher temperature is related with the dehydrogenation process of the AlCl$_3$-doped and un-doped LiNH$_2$-LiH composite samples.
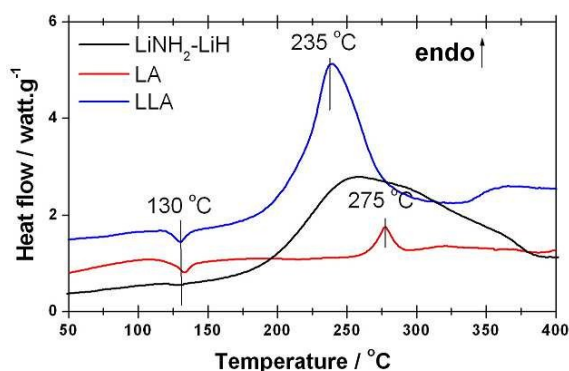

Figure 3. DSC curves of the LA and LLA samples. DSC curve of LiNH$_2$-LiH is shown as reference.

Evaluation of the DSC peaks of AlCl$_3$-doped and un-doped LiNH$_2$-LiH samples reveals that the dehydrogenation starts at the same temperature (about 180 °C), with a maximum at 235 and 275 °C, respectively, and finishes at different temperatures: 325 ºC (doped) and 385 °C (un-doped). In addition, the emission of ammonia is suppressed when AlCl$_3$ is added to LiNH$_2$-LiH.[22] Thus, a significant enhancement of dehydrogenation properties is achieved by AlCl$_3$ addition.

To clarify the nature of the thermal events, the LA sample was then heated under an argon and hydrogen atmospheres. The specimens obtained were characterized jointly by XRPD and FTIR. Figure 4 compares the XRPD patterns of the LA sample and LA heated at 150 °C under argon. An important improvement of the signal/background ratio and a peak sharpening can be observed starting with the LA sample (Fig. 4, bottom curve I). In fact, from Fig. 4 (curve II), a new set of peaks are evident at about 12.0, 17.0, 20.9 and 24.2°, which can be indexed together with the others, with a cubic unit cell of $I2_13$ space group, similarly to that proposed by Anderson et al. (Li$_4$(NH$_2$)$_3$Cl).[13] The entire XRPD pattern can be attributed to the formation of Li-Al-N-H-Cl phase,[23] with cell parameter a=10.446 Å. The rearrangement of the FCC disordered solid solution into a larger cubic cell is a consequence of the ordering process induced by heating at 150 °C and it is accompanied by heat evolution (exothermic peak at 130 ºC, Fig. 3).
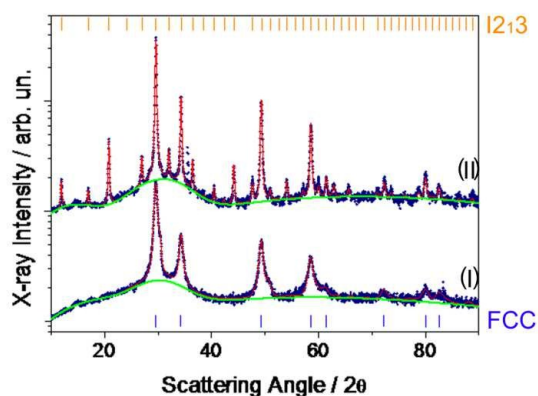

Figure 4. XRPD patterns of (I) LA sample (II) LA sample heated at 150 ºC under 0.1 MPa Ar for 0.5 h.
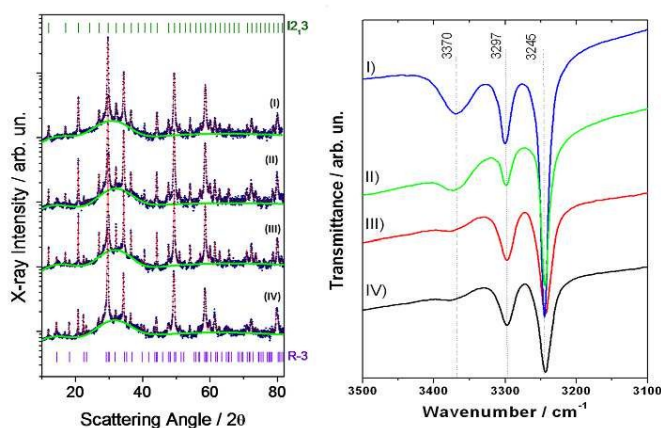
Figure 5. XRPD patterns (A) and FTIR spectra (B) of the LA sample after heating under 0.7 MPa of hydrogen pressure at: (I) 150 ºC, 0.5 h; (II) 300 ºC, 1 h; (III) 300 ºC, 5 h; (IV) 300 ºC, 12 h.

Figure 5 shows XRPD patterns of the LA sample after different thermal treatment under 0.7 MPa of hydrogen. In this figure the full lines are Rietveld fit of experimental data points where the fraction of Al ions were located in sites normally reserved for Lithium. However the structure (i.e., precise location and site occupancy of chemical species) cannot be solved unambiguously from X-ray patterns alone and neutron scattering experiments on the same mixtures where H atoms were replaced by deuterium are going to be investigated.

After thermal treatment of LA sample at 150 ºC under hydrogen (see Fig. 5A, curve I), a new sequence of peaks can be indexed as belonging with the cubic phase of the $I2_13$ space group analogous than that obtained after heating under argon (Fig. 4, curve II). Thermal treatment at 300 ºC for 1 h induces the incipient formation of a trigonal phase (extra peaks perceivable in curve II), which is isostructural with $Li_4(NH_2)_3Cl$ (R-3 space group). A detailed inspection of the XRPD patterns for the samples treated at 300 ºC for 5 and 12 h (Fig. 5, curves III and IV) shows the progressive emergency of the trigonal type-$Li_4(NH_2)_3Cl$ phase and a reduction of the amount of the cubic one. FTIR spectra of the as-heated LA sample under hydrogen at 150 and 300 ºC (Fig. 5B) confirm previous interpretations. After thermal treatment at 150 ºC, the shape of the bands at 3297 and 3245 cm^{-1} starts to become sharp, while those at 3315 and 3260 cm^{-1} associated with $LiNH_2$ are not clearly differentiated. The band intensity at 3370 cm^{-1} is reduced with thermal treatment,[28] being slightly detectable after heating at 300 ºC under hydrogen pressure for 12 h. A similar band was observed in the FTIR spectrum of $Li_7(NH_2)_6Br$ after heating at 200 ºC of the $LiNH_2$-MgH_2-0.05LiBr mixture.[17] According to our previous results from the $LiNH_2$-1.6LiH-xAlCl$_3$ composites,[23] the bands at 3297 and 3245 cm^{-1} can be associated with the cubic and trigonal type-$Li_4(NH_2)_3Cl$ phases, in agreement with XRPD results (Fig. 5A). As a remarkable result, N-H bands of the new amide-chloride phase were shifted to lower wave numbers than those of $LiNH_2$. This result indicates that the N-H bonds in the new amide-chloride are weakened, in consequence of the interaction of the amide-chloride with LiH. This also agrees with the thermal behaviour presented in Fig. 3.

These findings indicate that $LiNH_2$ reacts with $AlCl_3$ to produce first a FCC solid solution (reaction 4), which rearranges after heating at 150 ºC to form an amide-chloride phase isostructural with cubic-$Li_4(NH_2)_3Cl$ according to reaction (5):

$$3\ LiAl_x(NH_2)Cl_{3x} \xrightarrow{heating} 1/3\ Li_3Al_{3x}(NH_2)_3Cl_{9x}\ \text{with}\ x= 0.11 \quad (5)$$

These processes point out that the $Li_3Al_{3x}(NH_2)_3Cl_{9x}$ amide-chloride phase is a relatively stable phase derived from the Li-Al-N-H-Cl system. Similar interactions were observed during the formation of $Li_4(BH_4)(NH_2)_3$ by milling/heating of $LiBH_4$ with $LiNH_2$[29] or the formation of $Li_7(NH_2)_6Br$ by heating at 185 ºC of $LiNH_2$ and LiBr.[17] The presence of Al and Cl in the LA sample after thermal treatment under argon and hydrogen was confirmed by EDS analysis (see Fig. S3, ESI†). The average Al:Cl molar ratio was equal to 1:3, in agreement with the theoretical composition.

Dehydrogenation behaviour of amide-chloride phase with LiH addition.

In order to investigate the hydrogen storage properties of the as-milled $LiNH_2$-0.11AlCl$_3$ mixture with LiH addition, a comparative study between LA and LLA was developed using TG (Fig. 6A) and volumetric measurements (Fig. 6B), while the gases were analysed by FTIR. LA sample displays different steps in the TG curve (Fig. 6A), the first one starting at 95 ºC and reaching a relative mass change of 2.5% at 130 ºC. After this point, the relative mass loss increases up to 9.0% at 300 ºC. These mass changes are also observed in the derivative curve of TG as a function of time (Fig. S4 (ESI†)). Moreover, volumetric measurement for LA shows the onset temperature for dehydrogenation at about 130 ºC, being the total hydrogen released 2.0 wt% at 300 ºC. In accordance with TG and volumetric measurements, FTIR gas analysis confirms the evolution of NH_3 (Fig. S5 (ESI†)) at about 120 ºC during LA decomposition up to 300 ºC. In the case of the LLA sample, a slight hydrogen release starts at about 140 ºC and the hydrogen desorption rate grows with the temperature up to 235 ºC, in fair relation with the maximum of the endothermic peak in DSC (Fig. 3).
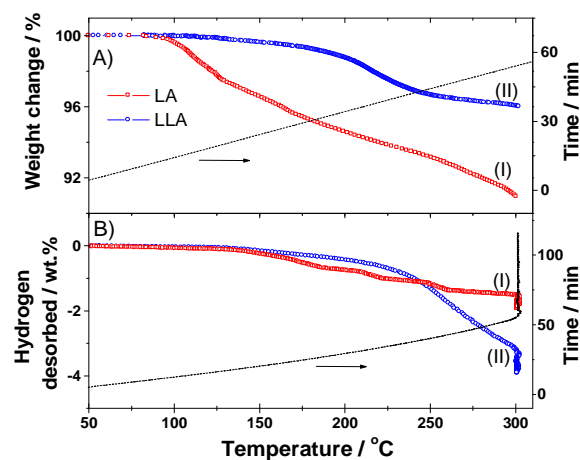

Figure 6. A) TG and B) hydrogen volumetric release curves of the LA and LLA samples. The arrow indicates the corresponding y axis of heating ramp.

There is a good accordance between relative mass change (<4.0 wt%) at 300 ºC and the hydrogen amount released (3.9 wt%) in Figs. 6A and 6B. This result is in agreement with the absence of ammonia release verified by gas-FTIR analysis.

To determine quantitatively the ammonia concentration in the desorbed gas up to 300 $^{\circ}$C, it was assumed that the released gas from $LiNH_2$-0.11AlCl$_3$ mixture contains x_1 mol H$_2$ and y_1 mol NH$_3$ (equations in ESI†). The calculated values of x_1 and y_1 are 0.15 and 0.18. Thus, the mole fraction of ammonia in the desorbed gas was about 54%. Similar estimation for the desorbed gas of the LiNH$_2$-1.6LiH-0.11AlCl$_3$ sample gives less than 0.03 mol% of ammonia. In fact, the relative mass change (<4.0 wt%) was practically equal to the amount of hydrogen released in the volumetric equipment (3.9 wt%) within the experimental error. Therefore, the ammonia released during dehydrogenation of the LLA sample is strongly suppressed by the addition of LiH.

To determine the nature of the phases after dehydrogenation in the volumetric equipment (Fig. 6B), samples were removed and analysed by XRPD and FTIR. Figure 7 shows the XRPD patterns of the samples obtained after decomposition of the LA (curve I) and LLA (curve II) samples. These patterns can be indexed as FCC like sequence of peaks, with a lattice parameter of 5.232 Å ($Fm\overline{3}m$ (1)) and 5.172 Å ($Fm\overline{3}m$ (2)) for LA and LLA, respectively. In the case of LLA sample, LiH phase is also detected. FTIR spectra provide additional evidence about the nature of phases (Fig. S6, ESI†). In both cases, a band in the region of imide phase is clearly identified, at 3155 and 3150 cm^{-1} for LA and LLA samples, respectively. Moreover, for LA sample additional bands at 3293 and 3240 cm^{-1} are also observed. This is an indication of the uncompleted decomposition of the LA sample. Probably, it is associated with the experimental set-up of the volumetric equipment, where gaseous species are not being released freely and they are partially accumulated due to flow mass controller restrictions.

To assess the reversibility of the LLA sample, the imide phase obtained after non-isothermal (Fig.6B, curve II) or isothermal (Fig. S7) dehydrogenation was submitted to hydrogen uptake under 0.7 MPa of hydrogen at 300 ºC. The material reabsorbs about 3.6 wt% in less than 10 min (Fig. S7). In Fig. 7 curve (III) the XRPD pattern of the rehydrogenated LLA sample is shown. The phases identified are both cubic and trigonal type-Li-Al-N-H-Cl phases and LiH, demonstrating the hydrogen storage reversibility of the LLA sample. It is noteworthy that the formation of amide-chloride phase is favoured during the heating of AlCl$_3$ doped LiNH$_2$-LiH under hydrogen pressure and its hydrogen desorption kinetics is better than that of un-doped Li-N-H (Figs. 3 and S7). In addition, the AlCl$_3$-doped sample resulted in significant suppression of ammonia release.
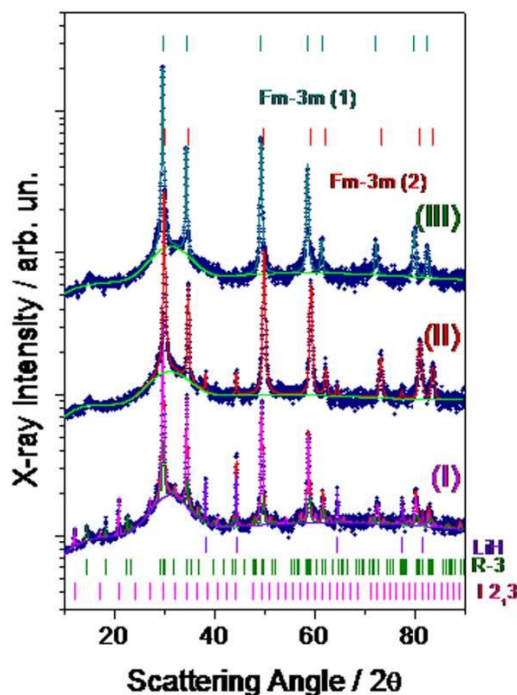
Figure 7. XRPD patterns after non-isothermal dehydrogenation up to 300 ºC in volumetric equipment for: (I) LA and (II) LLA samples. (III) LLA sample after rehydrogenation at 300 ºC under 0.7 MPa of hydrogen.

Conclusions

New phases in the Li-Al-N-H-Cl system, isostructural with previously observed cubic and trigonal type-Li$_4$(NH$_2$)$_3$Cl phases, were synthesized by a combination of milling and thermal treatment under different atmospheres (argon and hydrogen). The optimized process involves the milling of the LiNH$_2$-0.11AlCl$_3$ for 5 h with our experimental protocols under argon to form a FCC solid solution and subsequent thermal heating under argon at 150 ºC or under hydrogen pressure at 150-300 ºC. The rearrangement from the FCC to the amide-chloride phase could be related with an exothermic peak at 130 ºC in the DSC curve. In addition, the endothermic peaks at temperatures higher than 200 ºC were associated with the type-Li$_4$(NH$_2$)$_3$Cl phase decomposition. The typical FTIR spectrum of Li-Al-N-H-Cl phase was characterized and bands at 3297 and 3245 cm^{-1} were attributed to N-H stretches shifted in comparison with pure LiNH$_2$.

Decomposition pathway of the amide-chloride is dependent on the addition of the LiH phase. Heating of amide-chloride involves various steps with clear emission of ammonia and hydrogen from 120 to 300 ºC. The final product is an imide FCC phase, with 5.232 Å of lattice parameter. As a relevant result, when amide-chloride phase is heated in the presence of LiH, only hydrogen is released avoiding ammonia emission. The resultant material, an imide phase with FCC structure and lattice parameter 5.172 Å, is able to be rehydrogenated providing a new reversible hydrogen storage system.

Acknowledgements

References

1   G. Walker, Solid-state Hydrogen storage: Materials and Chemistry, Woodhead Publishing Limited, England, 2008.
2   P. Chen, Z. Xiong, J. Luo, J. Lin, L. T. Tan, *Nature* 2002, **420**, 302–304.
3   G. P. Meisner, M. L. Scullin, M. P. Balogh, F. E. Pinkerton, M. S. Meyer, *J. Phys. Chem. B* 2006, **110**, 4186-4192.
4   F. E. Pinkerton, M. S. Meyer, *J. Phys. Chem. C.* 2009, **113**, 11172-176.
5   Y. H. Hu, E. Ruckenstein, *J. Phys. Chem. A* 2003, **107**, 9737-39.
6   T. Ichikawa, N. Hanada, S. Isobe, H. Leng, H. Fujii, *J. Phys. Chem. B* 2004, **108**, 7887-92.
7   T. Ichikawa, S. Isobe, N. Hanada, H. Fujii, *J. Alloys Comp.* 2004, **365**, 271-276.
8   T. Ichikawa, N. Hanada, S. Isobe, H. Y. Leng, H. Fujii, *J. Alloys Compd.* 2005, **404-406**, 435-438.
9   Y. Kojima, Y. Kawai, *J. Alloys Compd.* 2005, **395**, 236-239.
10   S. Isobe, T. Ichikawa, K. Tokoyoda, N. Hanada, H. Leng, H. Fujii, et al., *Thermochim. Acta* 2008, **468**, 35-38.
11   J. Zhang, Y. H. Hu, *Ind. Eng. Chem. Res.* 2011, **50**, 8058–8064.
12   H. Leng, Z. Wu, W. Duan, G. Xia, Z. Li, *Int. J. Hydrogen Energy* 2012, **37**, 903–907.
13   P. A. Anderson, P. A. Chater, D. R. Hewett, P. R. Slater, *Faraday Discuss.* 2011, **151**, 271–284.
14   R. A. Davies, D. R. Hewett, P. A. Anderson, *Adv. Nat. Sci.: Nanosci. Nanotechnol.* 2015, **6**, 015005 (7 pp).
15   R. A. Davies, P. A. Anderson, *Int. J. Hydrogen Energy* 2015, **40,** 3001-3005.
16   W. I. F. David, M. O. Jones, D. H. Gregory, C. M. Jewell, S. R. Johnson, A. Walton, et al., *J. Am. Chem. Soc.* 2007**, 129**, 1594–1601.
17   B. Li, Y. Liu, C. Li, M. Gao, H. Pan, *J. Mat. Chem. A* 2014, **2**, 3155-62.
18   M. A. Howard, O. Clemens, P. R. Slater, P. A. Anderson, *J. Alloys Compd.* 2015, **645**, S174-S177.
19   R. A. Davies, D. R. Hewett, E. Korkiakoski, S. P. Thompson, P. A. Anderson, *J. Alloys Compd.* 2015, **645**, S343-S346.
20   H. Cao, G. Wu, Y. Zhang, Z. Xiong, J. Qiu, P. Chen, *J. Mater. Chem. A* 2014, **2**, 15816-822.
21   H. Cao, H. Wang, T. He, G. Wu, Z. Xiong, J. Qiu, P. Chen, *RSC Adv.* 2014, **4**, 32555-61.
22   L. Fernández Albanesi, P. Arneodo Lorochette, F. C. Gennari, *Int. J. Hydrogen Energy* 2013, **38**, 12325–34.
23   L. Fernández Albanesi, S. Garroni, P. Arneodo Larochette, P. Nolis, G. Mulas, S. Enzo, M. D. Baró, F. C. Gennari, *Int. J. Hydrogen Energy* 2015, **40**, 13506–17.
24   N. S. Gamba, P. Arneodo Larochette, F. C. Gennari, *RSC Adv.* 2015**,** 5**,** 68542-68550.
25   Maud - Materials Analysis Using Diffraction**,** http://maud.radiographema.com/ (accessed October 2015).
26   L. Lutterotti, *Nucl. Inst. Methods Phys. Res. B* 2010, **268**, 334–340.
27   J. W. Makepeace, M. O. Jones, S. K. Callear, P. P. Edwards, W. I. F. David, *Phys. Chem. Chem. Phys.* 2014, **16**, 4061–4070.
28   K. Nakamoto, *Infrared and Raman Spectra of Inorganic and Coordination Compounds*, Part B, 6th ed. 2009, Wiley, New York.
29   F. E. Pinkerton, G. P. Meisner, M. S. Meyer, M. P. Balogh, M. D. Kundrat, *J. Phys.Chem. B Let.* 2015, **109**, 6–8.

Ball Milling of the $LiNH_2$-$AlCl_3$ mixture after 5h conducts to the formation of a FCC solid solution. Its posterior heating at 150 ºC induces the production of an amide-chloride phase isostructural with cubic $Li_4(NH_2)_3Cl$. This Li-Al-N-H-Cl phase transforms into trigonal phase after heating at 300 ºC under H_2 pressure.

256x157mm (150 x 150 DPI)